energies

MDPI

Article

Thermoelectric Micro-Scale Generation by Carbonaceous Devices

Francesco Miccio

Istituto di Scienza e Tecnologia dei Materiali Ceramici CNR, via Granarolo 64, 48018 Faenza, Italy; francesco.miccio@cnr.it; Tel.: +39-0546-699774

Abstract: The paper reports on research focused on the use of largely available carbonaceous materials, such as graphite, carbon black and chars, as thermoelectric materials for micro-generation at high temperature. The key feature is the possibility to ignite the thermoelectric device to self-sustain electric generation. The results of the tests performed with such materials, under both cold and hot conditions, showed that a significant change of the electromotive force, with absolute increase up to three orders of magnitude, occurred under hot conditions with flame irradiation, achieving measured values of electromotive force up to 55 mV, in the best case. Monoliths based on biomass chars and covered with a layer of gunpowder gave rise to similar variation of the Seebeck coefficient, as the case of the flame exposed samples. This result confirms the basic idea of the investigation and the possibility of generating an electrical peak in a self-sufficient combustion thermoelectric device with power up to 1.0 W. A theoretical assessment has been proposed to provide an interpretation of the observed phenomenology, which is related to the non-linear dependence of the material properties on temperature, in particular the Seebeck coefficient and thermal conductivity.

Keywords: microgeneration; solid fuels; combustion; Seebeck effect

Citation: Miccio, F. Thermoelectric Micro-Scale Generation by Carbonaceous Devices. *Energies* **2022**, *15*, 8105. https://doi.org/10.3390/en15218105

Academic Editors: Amir Pakdel and David Berthebaud

Received: 21 September 2022
Accepted: 28 October 2022
Published: 31 October 2022

1. Introduction

Electric generation at micro-scale, with a characteristic size ranging from 10^{-1} to 10^2 mm and power of up to few Watts, could find application in several environments and fields, e.g., submarine, aerospace, biomedical, mechatronics, and robotics, when no possibility exists to use a conventional supply, such as batteries or photovoltaic generators. This kind of electric generation may be accomplished in different ways, such as micro engines/turbines [1], thermo-photovoltaic [2] or thermoelectric generators [3], piezoelectric devices [4], and others [5].

The thermoelectric, or Seebeck effect, is the generation of an electromotive force (EMF) throughout a solid element, when a temperature gradient occurs [6]. The interaction between the heat carriers in solid phase, i.e., phonons, and thermally excited electrons, leads to the accumulation of electrons and holes at the opposite sides of the solid element (e.g., a bar) with the generation of an electric field [7]. The ratio between generated EMF, measured in Volt or sub-multiples (mV and μV), and the temperature difference ΔT is defined as Seebeck coefficient (α) [8]. In general, metals have appreciable thermoelectric properties thanks to high electrical conductivity, whereas electrical insulators exhibit a very small Seebeck effect. For instance, platinum has an absolute Seebeck coefficients equal to −4.90 μV/K [9]. The Seebeck coefficient changes with temperature as a consequence of larger availability of thermally excited electrons in the conduction band [10]; for instance, the absolute Seebeck coefficient for Cu and Pt increases by 2–3 times with the temperature increase of a few hundred degrees [11].

The dimensionless figure of merit, $ZT = \alpha^2/(\rho\ k_t)$ [12] is calculated from the Seebeck coefficient, electrical resistivity (ρ), and thermal conductivity (k_t), representing the most relevant parameter for ranking a thermoelectric material/device. It is worth noting that ZT is inversely proportional to electrical resistivity and thermal conductivity.

Since graphite and carbons have substantially high electrical conductivity, they can exhibit a thermoelectric behavior. The Seebeck coefficient of carbon referred to Pt is positive and equal to +2.20 μV/K, being comparable to those of metals (e.g., Cu, Au, Ag ~7.20 μV/K), but remarkably lower than values of semi-conductors (e.g., Ge, Si ≥ 339 μV/K) [13]. In this respect, the micro-generation of flexible graphite layers was studied by Luo et al. [14], reporting an absolute thermoelectric power of −2.6 μV/K and highlighting the possibility of application at high temperature. Miccio [15] investigated the dependence of the Seebeck coefficient on the oxidation degree of graphite rods, as possible non-intrusive characterization of samples subjected to reactive or irradiating environments [16]. Biomass chars are also electrical conductors, provided that a high level of carbonization is achieved for decomposing their major constituents, i.e., lignin, hemicellulose, and cellulose [17]. Biomass chars exhibit moderate thermal conductivity in the range 0.15–0.40 W/m/K [18], thanks to their low density and extensive particle porosity. Furthermore, biomass chars are very reactive in oxidizing atmosphere if compared to fossil carbons, the activation energy for air gasification being in the range 70–90 kJ/mol [19] for biomass char, 100–140 kJ/mol for carbon black [20], and larger than 200 kJ/mol for graphite [21]. Finally, it is worth noting that all cited carbonaceous materials are very cheap with respect to metals like Ge and Si, or engineered materials (e.g., semi-conductors) normally used for thermoelectric application.

An experimental investigation on thermoelectric microgeneration by means of carbonaceous materials is presented in the article, with the aim to provide a stimulus to develop innovative devices for energy production under particular conditions with very low power (<1.0 W). A novel approach to the matter, namely the possible self-sustained conversion and generation upon the ignition of the thermoelectric device, is reported. The experimental results of the research are reported and discussed, along with a discussion based on fundamentals of thermoelectric generation.

2. Materials and Methods

2.1. Materials

The carbonaceous solids used during the tests were:

- graphite electrode (Gr);
- carbon black (CB);
- beech-wood char (BWC).

The graphite electrode was originally a rod with a diameter of 5 mm. In the case of the combustion tests, the graphite rod was worked with abrasive paper to obtain a thin lamina (5 × 80 mm) with thickness of about 1 mm. Carbon black (Degussa EB 158) was in the form of micrometric powder. Beech-wood char was obtained by coking beech rods at 800 °C in a tubular furnace for 30 min under N_2 atmosphere. BWC was used in bars (3 × 6 × 80 mm) or ground into powder with size less than 100 μm.

Powders of CB and BWC were mixed with pastry flour (00) and demineralized water to form a slurry that was casted in a silicon mold (5 × 10 × 70 mm) and cured in oven at 90 °C to obtain solid monoliths having similar dimensions. The relative mass ratios of flour were 1/5 and 1/2 for carbon black and beech-wood char, respectively, as consequence of the large difference in density between CB and BWC and the different workability of the resulting slurries.

Gunpowder was produced by mixing KNO_3 (Sigma Aldrich P8394), sulfur powder (Kollant 002297-011563) and BWC, by adopting the well-established formulation 75/10/15 %wt. respectively [22], then adding water and small amount of flour to form a slurry for coating some BWC monoliths and char bars.

Table 1 reports the density, porosity, and fixed carbon content of the three carbonaceous materials. Differences in density are attributable to the increased porosity of BWC with respect to Gr and CB. ICP-MS analysis evidenced the presence of major elements: Fe for graphite (0.12% by weight), and K for beech-wood char (0.02 by weight). In this respect,

Wei et al. [23] reported an enhancement of thermoelectric coefficient for carbon fibers in presence of iron oxide (Fe_2O_3).

Table 1. Properties of materials.

	Density g/mL	Porosity %	C Content % wt.
Graphite	1.62	14.6	99
Carbon black	1.80	-	97
Beech wood char	0.50	60.7	96

The electrical conductivity of all samples was measured at room temperature by means of a digital multimeter (Lafayette DMB-USB2). It resulted equal to 3.9×10^3 and $1.1 \times 10^2\ \Omega^{-1}m^{-1}$ for graphite and beech wood char, respectively. The electrical conductivity of casted monoliths from slurries was $17.0 \pm 1.0\ \Omega^{-1}m^{-1}$ for CB and $2.7 \pm 1.0\ \Omega^{-1}m^{-1}$ for BWC, samples having too low value (i.e., $<1.0\ \Omega^{-1}m^{-1}$) being rejected.

2.2. Experimental Apparatus

The experimental apparatus for thermoelectric tests is displayed in Figure 1. Two horizontal copper semi-cylindrical electrodes (1 and 2) at a distance of 60 mm sustained the sample (3). The copper purity is higher than 99% without traces of elements like Ni, Fe, Sn, Co, Mn, Zn, Ag, Au, Pt, as determined by an Energy-dispersive X-ray analysis performed at 20 keV. The contact surface was accurately cleaned before the test. Screwed clamps fastened the electrodes at both ends having care to not impart excessive stress in sample. Electrode 1 was heated by means of an electric resistance up to 130 °C by a low voltage DC supply (6). Electrode 2 was kept at room temperature. Two thermocouples (type K) were plugged into central holes of the electrodes for measuring the temperature in each element. The temperature difference between electrodes $\Delta T = T_1 - T_2$ was assumed as the reference driving force between hot and cold ends.

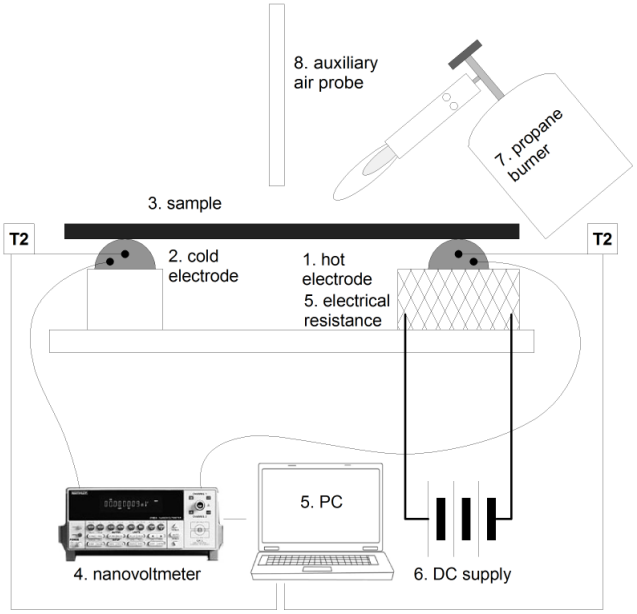

Figure 1. Experimental setup for thermoelectric measurements.

The probes of a Keithley 2182 A nano-voltmeter (4) were directly connected to the copper electrodes, taking care to avoid any junction with different conductors and keeping the contact area clean. Since the nano-voltmeter was serially connected with cold and hot electrodes with positive end at the hot side, it measured the opposite EMF of the

pair sample/Cu [7]. The measured EMF, in the order of hundreds of microvolts, and the temperatures T_1 and T_2 were acquired by a personal computer (5).

A propane burner (7) was used for the ignition/combustion tests with the flame applied to the middle of the sample. In some tests, an air stream of 1.0 L/min was supplied with a 4 mm probe after ignition to sustain the sample combustion. In most cases, these tests lasted until the collapse of the rod as a consequence of the local burn-off. The whole experimental setup was kept under a laboratory hood.

To calibrate the thermoelectric apparatus, a platinum lamina with purity 999/1000 was used as a reference specimen before each test.

3. Results

The measured values of electromotive force and temperature were worked out into absolute Seebeck coefficient (α), calculated via Equation (1) derived from Kockert et al. [24] upon changing the reference metal from Pt to Cu, where $\Delta T = T_1 - T_2$ and $\Delta V = V_1 - V_2$ are the average measured temperature and voltage differences over the test time, typically 5′. The coefficient 2.6 μV/K is the absolute Seebeck coefficient of copper [14].

$$\alpha = 2.6 - \Delta V/\Delta T \ [\mu V/K] \quad (1)$$

The measurement errors due to presence of impurities in the electrodes and wires were estimated to be lower than 2% by calibration of the equipment with 999/1000 purity Pt lamina. The errors of the temperature readings (±1.0 K) and voltage measurement (<1.0 μV) give rise to uncertainties in determination of α lower than 5.0%, at typical test conditions, i.e., in presence of $\Delta T \geq 100$ K.

A typical time profile of EMF recorded during a test with flame is shown in Figure 2 for a BWC bulk. The measured voltage that was negative both at room temperature suddenly decreased, achieving a minimum value of about 2230 μV when the flame was applied to the sample. It is worth noting that an inversion of the generated EMF at high temperature, e.g., from negative to positive level, could also occur depending on the predominant mechanism of electrical conduction at different temperature, switching from hole-like (p-type) to electron-like (n-type) behavior [20]. The sample collapsed at around time 270 s and some negative peaks before collapse may be attributable to occurrence of local breaks in the sample structure during conversion.

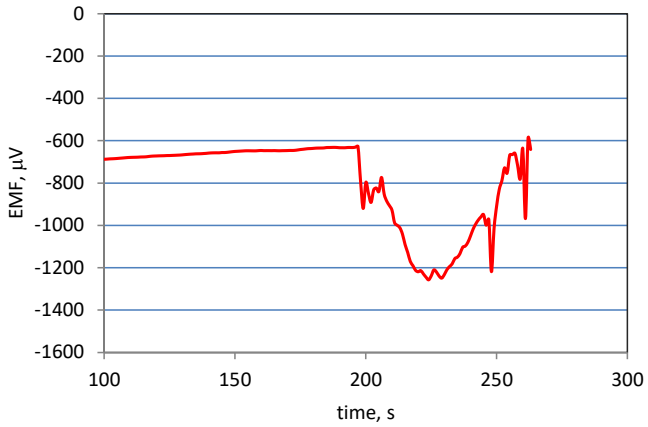

Figure 2. Time profile of measured EMF during a test with BWC bulk and flame from t = 200 to t = 260 s (T_1 = 143.7 ± 2.0 °C, T_2 = 42.5 ± 4.9 °C).

Figure 3 shows snapshots taken during tests with flame ignition for three different samples, graphite, beech wood bulk and beech wood monolith. Graphite lamina (Figure 3A) did not ignite, even if the flame was applied for several seconds and supplemental air flow (200 L/min) was blown. The lamina became red for the high temperature induced by the flame and correspondingly a small change in EMF was recorded as reported in Table 2.

Nevertheless, there was no evidence of combustion of the sample, whose shape did not change after the test.

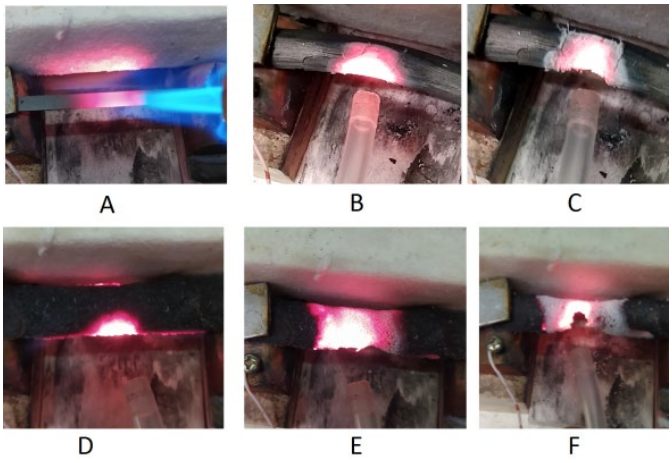

Figure 3. Snapshots of samples subjected to ignition: graphite lamina (**A**); BWC bulk (**B**,**C**); BWC monolith (**D**–**F**). In tests (**B**–**F**) air stream supplied upon ignition.

Table 2. Absolute Seebeck coefficients (μV/K).

Sample	No Flame	with Flame	abs. Change
Gr lamina	0.10	−1.73	1.83
CB monolith	3.18	4.70	1.52
BWC bulk	8.80	14.9	6.10
BWC bulk + gunpowder	8.00	15.6	11.6
BWC monolith	12.4	54.6	42.2
BWC monolith + gunpowder	11.9	528	516

Conversely, BWC bulk (Figure 3B,C) promptly ignited after contact with the flame and the sample combustion was sustained by the supplemental air flow. The test ended with the collapse of the sample by complete conversion in the middle section. Similarly, BWC monolith (Figure 3D–F) was ignited and the combustion occurred in the middle until collapse of the monolith. Tests were also performed with carbon black monoliths but did lead to stable ignition, reproducing a behavior similar to graphite, because of kinetic limits.

Figure 4 shows three snapshots from a test with CB monolith that was coated by a layer of gunpowder in the middle. The gunpowder ignition was very fast (Figure 4A) and followed by a few seconds of self-sustained combustion of gunpowder (Figure 4B). However, upon extinguishment of gunpowder, the monolith did not get ignited (Figure 4C). The transient behavior was reflected in the measured EMF signal that exhibited a negative and intense peak up to 250 mV (absolute value) occurred during the combustion of gunpowder.

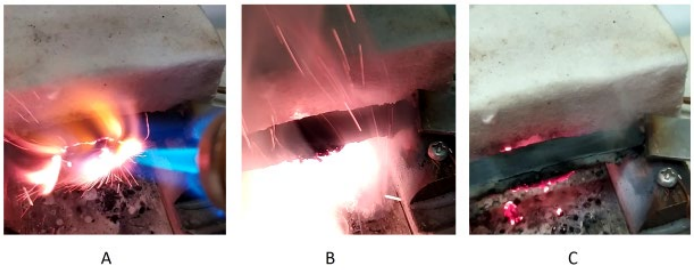

Figure 4. Snapshots of CB monolith subjected to ignition in presence of gunpowder: ignition with flame (**A**); self-sustained combustion (**B**); extinction (**C**).

Similar tests were carried out with both BWC bulk and monolith covered by gunpowder. The recorded signal of EMF is shown in Figure 5A, where the negative peak following gunpowder ignition achieved an absolute value of around 1750 μV at time 210 s. Conversely, a much larger negative peak up to −55,000 μV (Figure 5B) was achieved with BWC monolith. Both samples showed incipient combustion after the gunpowder flame. It is worth noting that such tests Figure 5 did not occur in the presence or air blowing, so the combustion quickly extinguished. Anyway, the reported profiles of Figure 5 suggest that a large EMF impulse can be obtained under such conditions.

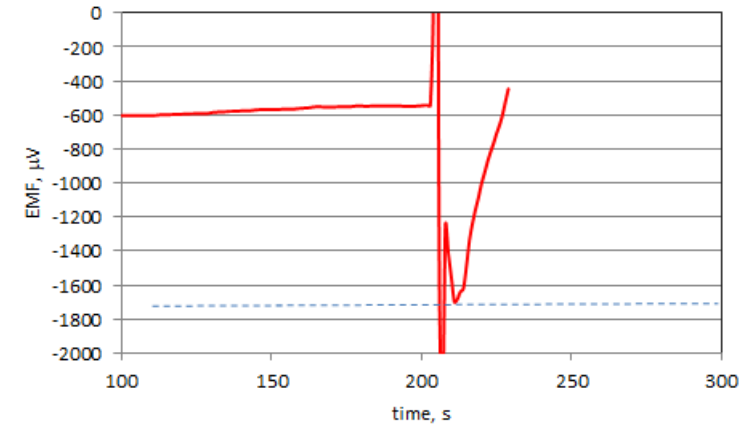

(**A**)

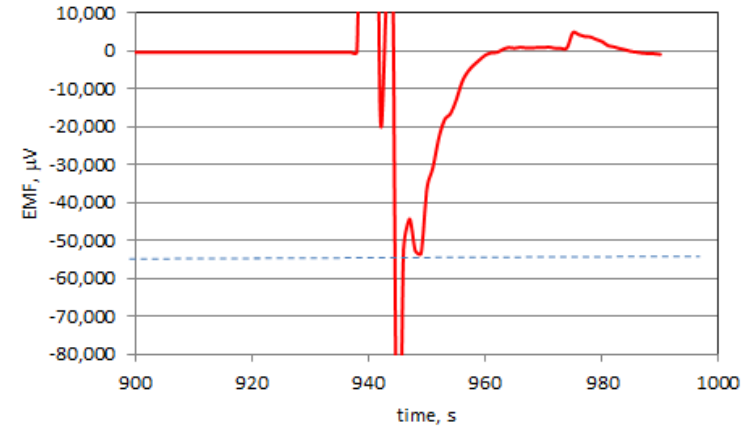

(**B**)

Figure 5. Time profile of EMF during tests of gunpowder ignition with (**A**) BWC bulk (T_1 = 132.2 ± 14 °C, T_2 = 34.0 ± 1.1 °C) and (**B**) BWC monolith covered by gunpowder (T_1 = 144.7 ± 1.6 °C, T_2 = 40.7 ± 2.9 °C).

The results of tests carried out with all samples are summarized in Table 2, as absolute Seebeck coefficient computed via Equation (1). Graphite, CB monolith and BWC bulk exhibited little changes of their thermoelectric figure moving from room temperature to flame exposition, the variation being lower than 10 μV/K.

The results were very different for BWC monolith that gave rise to large variation of the absolute Seebeck coefficient with change of about four times, moving from 12.4 to 54.6 μV/K. The intrinsic composite nature of the BWC monolith that is based on a binder/filler structure could explain this finding, Composite or doped materials, like semi-conductors, are known to exhibit improved thermoelectric effects, some orders of magnitude higher than common materials (e.g., metals), because they have modified properties, namely high electrical conductivity and low lattice thermal conductivity [25]. In a

composite monolith, differential changes of the transport properties may occur at increasing temperature, with consequent increment of the thermoelectric coefficient.

The BWC bulk and monolith covered with a layer of gunpowder gave rise to similar variation of the Seebeck coefficient, as the case of the flame exposed samples. In both cases di absolute change of α was higher with respect to tests without gunpowder, i.e., 11.6 and 516 for BWC bulk and monolith, respectively, the higher temperature reached during the transient gunpowder burning explaining this result.

The analysis of the investigated devices suggests they should be based on:

1. a reactive carbon to easily achieve device ignition;
2. additive for obtaining a composite structure that enhances the device performance;
3. cheap components because of disposable operation of the device;
4. presence of a pyrotechnic layer to promote the ignition.

4. Discussion

The experimental results demonstrated that coupling regions at different temperatures, i.e., low temperature near electrodes and high temperature in the center, leads to increase the electromotive force. This effect is theoretical assessed in the following.

For a single element having homogeneous properties the equations of combined heat flux Q and electricity carriers current I in uniaxial x system are given by Equations (2) and (3) [26], where k, Π, and ρ are thermal conductivity, Peltier coefficient and electrical resistivity.

$$Q = -k\, dT/dx + \Pi\, I \tag{2}$$

$$-dV/dx = \rho\, I + \alpha\, dT/dx \tag{3}$$

Under the hypothesis open electric circuit (I = 0) Equations (2) and (3) are simplified in Equations (4) and (5).

$$Q = -k\, dT/dx \tag{4}$$

$$-dV/dx = \alpha\, dT/dx \tag{5}$$

Integration of Equations (4) and (5) leads to:

$$Q = -k\, \Delta T/\Delta x \tag{6}$$

$$\Delta V = -\alpha\, \Delta T \tag{7}$$

Let consider a composite device formed by three zones in series (1, 2 and 3). Equations (6) and (7) may be applied to each zone:

$$Q = -k_1\, \Delta T_1/\Delta x_1 = -k_2\, \Delta T_2/\Delta x_2 = -k_1\, \Delta T_1/\Delta x_1 = -k_3\, \Delta T_3/\Delta x_3 \tag{8}$$

$$\Delta V = -(\alpha_1\, \Delta T_1 + \alpha_2\, \Delta T_2 + \alpha_3\, \Delta T_3) \tag{9}$$

where Equation (8) expresses the continuity of the heat flux and Equation (9) gives the sum of EMFs in each zone for a series connection. Under the hypothesis that zones 1 and 3 have same properties, length and ΔT, following Equation (10) may be derived, where y is the fraction of the total length ΔX occupied by intermediate zone 2.

$$\frac{\Delta V}{\Delta T} = -\frac{(1-y)\frac{\alpha_1}{k_1/k_2} + y\alpha_2}{\frac{1-y}{k_1/k_2} + y} \tag{10}$$

For given values of Seebeck coefficient and thermal conductivity, Equation (10) provides the dependence of the overall Seebeck coefficient for the composite devices. It is worth noting that Equation (8) is a continuity equation taking into account only conduction, and omitting the contribution of convection and radiation to heat transfer, which is a rough

simplification in current preliminary approach. Furthermore, the thermal conductivity of zones 1 and 2 are not relevant, since they appear as ratio in Equation (10).

Figure 6 shows the dimensionless overall coefficient α^* obtained for three k_1/k_2 ratios and $\alpha_1/\alpha_2 = 1/100$. The points along the diagonal (diamonds) are obtained for $k_1 = k_2$; in such case the overall Seebeck coefficient of the composite device equals the average value computed over y. More interestingly, if the thermal conductivity of the zones are different, there is a non-linear dependence of α^* on y and the position of the curve is over (under) the diagonal if k_2 is lower (greater) than k_1.

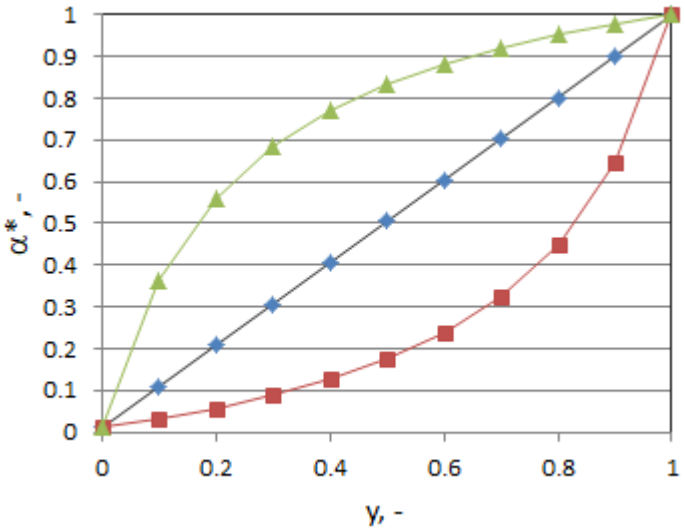

Figure 6. Change of the dimensionless Seebeck coefficient with the extent of the intermediate zone for three k_1/k_2 ratios: diamonds $k_1/k_2 = 1$; squares $k_1/k_2 = 1/5$; triangles $k_1/k_2 = 5/1$. $\alpha_1/\alpha_2 = 1/100$.

Results of Figure 6 provides a reasonable explanation of observed phenomena because when the central zone of the device is heated the local Seebeck coefficient is likely increased by the temperature [11,15] and the thermal conductivity may decrease, also as consequence of carbon oxidation [27]. The combined effect of both changes leads to a drastic increase of the Seebeck coefficient (triangles in Figure 6 corresponding to $k_1/k_2 = 5$).

5. Conclusions

The experimental tests confirm the concept correctness, i.e., the possibility of generating an electromotive force by means of a self-burning thermoelectric device based on very cheap and disposable carbonaceous materials.

Tests performed with gunpowder combustion gave rise to a large EMF impulse, up to 55 mV (absolute), indicating that the self-burning thermoelectric device can be exploited for micro-generation. Use of biomass char is beneficial for such scope, owing to high oxidation reactivity and low thermal conductivity.

Apart from the effect of impurities or composite nature of the material, the synergy of changes in thermal conductivity and Seebeck coefficient at high temperature upon ignition would be the main factor influencing the drastic increase of measured EMF during the transient test.

The simple mathematical model provides qualitative confirmation of experimental findings, provided that the material properties changes with temperature in direction of emphasizing the thermoelectric effect: increase of local Seebeck coefficient, and decrease of thermal conductivity.

Even if the efficiency of conversion is likely to be very low, the optimization of the choice of materials and design of the device, also considering multiple modules in stacks, could allow achieving better performance in terms of generated EMF, power, and efficiency.

Funding: This research received no external funding.

Data Availability Statement: Not applicable.

Acknowledgments: G.P. Beretta is gratefully acknowledged for the fruitful discussion about the concept and the development of the research.

Conflicts of Interest: The author declares no conflict of interest.

Nomenclature

EMF	electromotive force
k	thermal conductivity
I	current
Q	heat flux
T	temperature
V	voltage
x	axial coordinate
y	length fraction
ZT	figure of merit, -
Greek symbols	
α	Seebeck coefficient
Π	Peltier coefficient
ρ	electrical resistivity

References

1. Jurado-Sánchez, B.; Wang, J. Micromotors for environmental applications: A review. *Environ. Sci. Nano* **2018**, *5*, 1530–1544. [CrossRef]
2. Bitnar, B. Silicon, germanium silicon/germanium photocells for thermophotovoltaics applications. *Semicond. Sci. Techol.* **2003**, *18*, S221–S227. [CrossRef]
3. Merotto, L.; Fanciulli, C.; Dondè, R.; De Iuliis, S. Study of a thermoelectric generator based on a catalytic premixed meso-scale combustor. *Appl. Energy* **2016**, *162*, 346–353. [CrossRef]
4. Siddique, A.M.; Mahmud, S.; Van Heyst, B. A comprehensive review on vibration based micro power generators using electromagnetic and piezoelectric transducer mechanisms. *Energy Convers. Manag.* **2015**, *106*, 728–747. [CrossRef]
5. Fernandez-Pello, A.C. Micropower generation using combustion: Issues and approaches. *Proc. Combust. Inst.* **2002**, *29*, 883–899. [CrossRef]
6. Condon, E.U.; Odishaw, H. *Handbook of Physics*; McGraw–Hill: New York, NY, USA, 1958.
7. Tilley, R.J.D. *Principles and Apllications of Chemical Defects*; Stanley Thornes Ltd.: Chetenham, UK, 1998.
8. Rowe, D.M. *Thermoelectrics Handbook: Macro to Nano*; Taylor & Francis: Milton Park, UK, 2005.
9. Amagai, Y.; Shimazaki, T.; Okawa, K.; Fujiki, H.; Kawae, T.; Kaneko, N.-H. Precise measurement of absolute Seebeck coefficient from Thomson effect using ac-dc technique. *AIP Adv.* **2019**, *9*, 065312. [CrossRef]
10. Cox, P.A. *The Electronic Structure and Chemistry of Solids*; Oxford University Press: Oxford, UK, 1987.
11. Reed, R.P. Thermal Effects in Industrial Electronic Circuits. In *The Industrial Electronics Handbook*; Irwin, J.O., Ed.; CRC Press LLC: Boca Raton, FL, USA, 1997; pp. 151–163.
12. Snyder, G.J.; Snyder, A.H. Figure of merit ZT of a thermoelectric device defined from materials properties. *Energy Environ. Sci.* **2017**, *10*, 2280–2283. [CrossRef]
13. Cardarelli, F. *Materials Handbook*; Springer: Berlin/Heidelberg, Germany, 2008.
14. Luo, X.C.; Chugh, R.; Biller, B.C.; Hoi, Y.M.; Chung, D.D.L. Electronic applications of flexible graphite. *J. Electron. Mater.* **2002**, *31*, 535–544. [CrossRef]
15. Miccio, F. Thermoelectric properties of carbonaceous solids. *Carbon Lett.* **2016**, *19*, 107–111. [CrossRef]
16. Acosta, B.; Sevini, F. Evaluation of irradiation damage effect by applying electric properties based techniques. *Nucl. Eng. Des.* **2004**, *229*, 165–173. [CrossRef]
17. Collard, F.-X.; Blin, J. A review on pyrolysis of biomass constituents: Mechanisms and composition of the products obtained from the conversion of cellulose, hemicelluloses and lignin. *Renew. Sustain. Energy Rev.* **2014**, *38*, 594–608.
18. Mason, P.E.; Darvell, L.I.; Jones, J.M.; Williams, A. Comparative Study of the Thermal Conductivity of Solid Biomass Fuels. *Energy Fuels* **2016**, *30*, 2158–2163. [CrossRef] [PubMed]
19. Di Blasi, C.; Buonanno, F.; Branca, C. Reactivities of some biomass chars in air. *Carbon* **1999**, *37*, 1227–1238. [CrossRef]
20. Sharma, H.N.; Pahalagedara, L.; Joshi, A.; Suib, S.L.; Mhadeshwar, A.B. Experimental Study of Carbon Black and Diesel Engine Soot Oxidation Kinetics Using Thermogravimetric Analysis. *Energy Fuels* **2012**, *26*, 5613–5625. [CrossRef]

21. Laurendeau, N.M. Heterogeneous kinetics of coal char gasification and combustion. *Prog. Energy Combust. Sci.* **1978**, *4*, 221–270. [CrossRef]
22. Ritchie, T.S.; Riegner, K.E.; Seals, R.J.; Rogers, C.J.; Riegner, D.E. Evolution of Medieval Gunpowder: Thermodynamic and Combustion Analysis. *ACS Omega* **2021**, *6*, 22848–22856. [CrossRef] [PubMed]
23. Wei, J.; Hao, L.; He, G.P.; Yang, C.L. Enhanced thermoelectric effect of carbon fiber reinforced cement composites by metallic oxide/cement interface. *Ceram. Int.* **2014**, *40*, 8261–8263. [CrossRef]
24. Kockert, M.; Kojda, D.; Mitdank, R.; Mogilatenko, A.; Wang, Z.; Ruhhammer, J.; Kroener, M.; Woias, P.; Fischer, S.F. Nanometrology: Absolute Seebeck coefficient of individual silver nanowires. *Sci. Rep.* **2019**, *9*, 20265. [CrossRef] [PubMed]
25. Odahara, H.; Yamashita, O.; Satou, K.; Tomiyoshi, S.; Tani, J.-i.; Kido, H. Increase of the thermoelectric power factor in Cu/Bi/Cu, Ni/Bi/Ni, and Cu/Bi/Ni composite materials. *J. Appl. Phys.* **2005**, *97*, 103722. [CrossRef]
26. Kjelstrup, S.; Bedeaux, D. *Non-Equilibrium Thermodynamics of Heterogeneous Systems*; World Scientific: Singapore, 2008; Volume 16, p. 452.
27. Zhang, X.; Dukhan, A.; Kantorovich, I.I.; Bar-Ziv, E. The Thermal Conductivity and Porous Structure of Char Particles. *Combust. Flame* **1998**, *113*, 519–531. [CrossRef]